^{20}Ne + ^{76}Ge elastic and inelastic scattering at 306 MeV

A. Spatafora,[1,2,*] F. Cappuzzello,[1,2,†] D. Carbone,[1] M. Cavallaro,[1] J. A. Lay,[3,4] L. Acosta,[5] C. Agodi,[1] D. Bonanno,[6] D. Bongiovanni,[1] I. Boztosun,[7] G. A. Brischetto,[1,2,8] S. Burrello,[1] S. Calabrese,[1,2] D. Calvo,[9] E. R. Chávez Lomelí,[5] I. Ciraldo,[1,2] M. Colonna,[1] F. Delaunay,[10,9,11] N. Deshmukh,[1] J. L. Ferreira,[12] P. Finocchiaro,[1] M. Fisichella,[9] A. Foti,[6] G. Gallo,[1,2] A. Hacisalihoglu,[1,13] F. Iazzi,[9,11] G. Lanzalone,[1,14] H. Lenske,[15] R. Linares,[12] D. Lo Presti,[2,6] J. Lubian,[12] M. Moralles,[16] A. Muoio,[1] J. R. B. Oliveira,[17] A. Pakou,[18] L. Pandola,[1] H. Petrascu,[19] F. Pinna,[9,11] S. Reito,[6] G. Russo,[2,6] G. Santagati,[1] O. Sgouros,[1] S. O. Solakci,[7] V. Soukeras,[1] G. Souliotis,[20] D. Torresi,[1] S. Tudisco,[1] A. Yildirim,[7] and V. A. B. Zagatto[17]
(for the NUMEN Collaboration)

[1]*Istituto Nazionale di Fisica Nucleare, Laboratori Nazionali del Sud, I-95125 Catania, Italy*
[2]*Dipartimento di Fisica e Astronomia "Ettore Majorana", Università di Catania, I-95125 Catania, Italy*
[3]*Departamento de Física Atómica Molecular y Nuclear, Universidad de Sevilla, E-41080 Sevilla, Spain*
[4]*Instituto Interuniversitario Carlos I de Física Teórica y Computacional (iC1), E-41080 Sevilla, Spain*
[5]*Instituto de Física, Universidad Nacional Autónoma de México, 04510 México City, México*
[6]*Istituto Nazionale di Fisica Nucleare, Sezione di Catania, I-95125 Catania, Italy*
[7]*Akdeniz University, 07070 Antalya, Turkey*
[8]*Centro Siciliano di Fisica Nucleare e Struttura della Materia, I-95125 Catania, Italy*
[9]*Istituto Nazionale di Fisica Nucleare, Sezione di Torino, I-10125 Torino, Italy*
[10]*Laboratoire de Physique Corpuscolaire de Caen, Normandie Université, ENSICAEN, UNICAEN, CNRS/IN2P3, F-14000 Caen, France*
[11]*Dipartimento Scienza Applicata e Tecnologia, Politecnico di Torino, I-10129 Torino, Italy*
[12]*Instituto de Fisica, Universidade Federal Fluminense, 24210-340 Niteroi, Brazil*
[13]*Institute of Natural Science, Karadeniz Teknik Universitesi, 61080 Trabzon, Turkey*
[14]*Università degli Studi di Enna "Kore", 94100 Enna, Italy*
[15]*University of Giessen, 35390 Giessen, Germany*
[16]*Instituto de Pesquisas Energeticas e Nucleares IPEN/CNEN, 05508-000 São Paulo, Brazil*
[17]*Instituto de Fisica, Universidade de São Paulo, 05508-090 São Paulo, Brazil*
[18]*Department of Physics, University of Ioannina and Hellenic Institute of Nuclear Physics, 451 10 Ioannina, Greece*
[19]*Institutul National de Cercetare-Dezvoltare pentru Fizica si Inginerie Nucleara Horia Hulubei, 077125 Bucarest, Romania*
[20]*Department of Chemistry, University of Athens and Hellenic Institute of Nuclear Physics, 157 72 Athens, Greece*

(Received 18 July 2019; published 30 September 2019)

Background: Double charge exchange (DCE) nuclear reactions have recently attracted much interest as tools to provide experimentally driven information about nuclear matrix elements of interest in the context of neutrinoless double-β decay. In this framework, a good description of the reaction mechanism and a complete knowledge of the initial and final-state interactions are mandatory. Presently, not enough is known about the details of the optical potentials and nuclear response to isospin operators for many of the projectile-target systems proposed for future DCE studies. Among these, the ^{20}Ne + ^{76}Ge DCE reaction is particularly relevant due to its connection with ^{76}Ge double-β decay.

Purpose: We intend to characterize the initial-state interaction for the ^{20}Ne + ^{76}Ge reactions at 306 MeV bombarding energy and determine the optical potential and the role of the couplings between elastic channel and inelastic transitions to the first low-lying excited states.

Methods: We determine the experimental elastic and inelastic scattering cross-section angular distributions, compare the theoretical predictions by adopting different models of optical potentials with the experimental data, and evaluate the coupling effect through the comparison of the distorted-wave Born approximation calculations with the coupled channels ones.

Results: Optical models fail to describe the elastic angular distribution above the grazing angle ($\approx$9.4°). A correction in the geometry to effectively account for deformation of the involved nuclear systems improves the agreement up to about 14°. Coupled channels effects are crucial to obtain good agreement at large angles in the elastic scattering cross section.

*alessandro.spatafora@lns.infn.it
†cappuzzello@lns.infn.it

Conclusions: The analysis of elastic and inelastic scattering data turned out to be a powerful tool to explore the initial and final-state interactions in heavy-ion nuclear reactions at high transferred momenta.

DOI: 10.1103/PhysRevC.100.034620

I. INTRODUCTION

The study of single (SCE) and double charge exchange (DCE) reaction cross sections induced by heavy projectiles has recently attracted much interest because of the possible connection with double-β decay [1]. In particular, the NUMEN (Nuclear Matrix Elements for Neutrinoless double-β decay) and NURE (NUclear REactions for neutrinoless double-β decay) projects at the Laboratori Nazionali del Sud of the Istituto Nazionale di Fisica Nucleare (LNS-INFN) [2,3] aim to extract relevant information regarding nuclear structure of neutrinoless double-β decay ($0\nu\beta\beta$) nuclear matrix elements (NME) by measuring cross sections of DCE and SCE. Other complementary studies at RIKEN (RIkagaku KENkyūsho, in english National Institute of Physical and Chemical Research, Tokyo) [4,5] and RCNP (Research Center for Nuclear Physics, Osaka University) [6] have recently focused on DCE reactions not only in relation to $0\nu\beta\beta$ but also to populate exotic structures. Theoretical indications suggest that not only the transition to the ground state of the daughter nucleus in $0\nu\beta\beta$, accessed by DCE reaction, but also the whole double Gamow-Teller strength could, in principle, be connected to $0\nu\beta\beta$-NME [7].

This task demands that a detailed microscopic description of the reaction mechanism is accomplished. The state-of-art reaction theory for the description of SCE and DCE reactions up to high excitation energy triggers the need for knowledge of initial and final-state interactions associated to the involved beams, e.g., ^{12}C, ^{18}O, and ^{20}Ne, at energies from 10 to 60 MeV/u and the heavy targets of interest for the NUMEN purposes. The information about the optical potential for such systems in this energy regime is limited and not deeply tested. This task in turn requires the control of the distortions of the incoming and outgoing waves due to the optical potentials, as shown in Refs. [8–10].

Optical potentials play a central role in heavy-ion quantum scattering theory, as they describe the average interaction during the collisions between the nuclei involved in the entrance and exit partitions. The complete many-nucleon scattering is a challenging problem. Very recently, *ab initio* reaction theory [11] has been shown to be a promising theory but still limited to light nuclear systems with few reaction channels open. The complexity of the many-body scattering problem of heavy nuclei can be carried out to a calculable scheme by the choice of an appropriate model space for the nuclear wave functions, with the caveat that the space left out from the model is effectively accounted by the introduction of a complex polarization potential [12]. Such a procedure has been commonly used to analyze atomic nuclei elastic and inelastic scattering such as reaction channels. For the latter, the optical potential is complemented by a perturbative potential, describing the specific nuclear transitions feeding the selected outgoing channel.

A typical way to determine the optical potential is to use parametrizations of Woods-Saxon shape adjusted to reproduce experimental elastic scattering cross sections at the appropriate incident energy and momentum transfer for the nuclear systems involved in both the incoming and outgoing channels. Despite its simplicity, this procedure hides the role of internal degrees of freedom of the projectile and target nuclei. Potentials obtained by folding the *frozen* densities of the colliding nuclei with a realistic nucleon-nucleon interaction are expected to be successful models of the optical potentials. This is mainly due to the strong absorption which confines the reaction source close to the surfaces of the colliding systems, making the system less sensitive to the internal regions where the overlap between projectile and target can change significantly the densities from the assumed frozen condition [13]. Although there are several references [14,15] on the general topic, to our knowledge, no data exist at a beam energy of about 15 AMeV and no theoretical studies have been published concerning the case of ^{20}Ne beam, which is one of the main probes for NUMEN.

A deeper understanding of the scattering dynamics can be achieved using the *coupled channels* (CC) method, in which relevant internal states of the projectile-target systems are explicitly taken into account. An interesting application of the CC analysis is the recent search for nuclear structure effects in $^{12}\mathrm{C} + {}^{12}\mathrm{C}$, $^{16}\mathrm{O} + {}^{16}\mathrm{O}$ at energies around the Coulomb barrier up to 1.5 GeV, where the complex diffractive patterns observed in the angular distributions were ascribed to couplings of elastic channel with 2^+, 3^-, and 4^+ low-lying excited states [16,17]. Similar results are found in $^{16}\mathrm{O} + {}^{27}\mathrm{Al}$ and $^{16}\mathrm{O} + {}^{60}\mathrm{Ni}$ elastic and inelastic cross-section data [18–21], where the important roles of nuclear surface deformation and coupling with inelastic transitions and transfer reactions are also discussed. The main picture is that CC effects are relevant, especially when the interest is in low cross-section data, as elastic scattering at large angles or suppressed transitions in the reaction channels.

This work is part of the network of reactions studied in the same experiment performed at the LNS-INFN within the NUMEN project with the goal to extract the cross section of the $^{76}\mathrm{Ge}(^{20}\mathrm{Ne}, {}^{20}\mathrm{O})^{76}\mathrm{Se}$ DCE reaction. Elastic and inelastic scattering data for the system $^{20}\mathrm{Ne} + {}^{76}\mathrm{Ge}$ at 15.3 AMeV are here shown. The experimental setup and the data reduction technique are described in the next sections. The analysis was performed in the optical model (OM) framework through the introduction of several optical potentials in the CC approach. Results obtained with Woods-Saxon-like potential following the Akyuz-Winther systematics [22,23] and double-folding potentials are compared to the data. In particular, two different double-folding potentials are used: the São Paulo [24,25] potential and a double folding potential using the T-matrix free nucleon-nucleon interaction [26,27]. The effect of lowest order truncation to a single channel, known as the distorted-wave Born approximation (DWBA) and the inclusion of relevant low-lying excited states, is studied and a comparison of this results with the CC ones will be shown.

II. EXPERIMENT AND DATA REDUCTION

A beam of $^{20}Ne^{4+}$ ions was accelerated to 306 MeV by the LNS-INFN superconducting cyclotron [28], fully stripped by crossing a thin carbon foil and transported to the target position, located at the object point of the MAGNEX large acceptance magnetic spectrometer [29]. The target consisted of a 390 ± 40 μg/cm^2 ^{76}Ge layer, 98% enriched, evaporated onto a 56 ± 6 μg/cm^2 carbon backing. A copper Faraday cup with 0.8 cm entrance diameter and 3 cm deep mounted 15 cm downstream of the target was used to stop the beam and collect its charge. An electron suppressor polarized at -200 V and a low noise charge integrator allowed a charge collection accuracy of better than 10% in all the experiment runs.

The ^{20}Ne ejectiles, produced in the projectile-target collisions, were analyzed for momentum in five different runs in which the optical axis of MAGNEX was oriented, compared to the beam direction, at $\theta_{opt} = 8^\circ$, 13°, 16°, and 19°. In four of them, at each angle, the MAGNEX solid angle acceptance was set to 50 msr by means of slits at the entrance of the spectrometer. At $\theta_{opt} = 8^\circ$, due to the high elastic cross section at forward angles, the beam current was optimized at about 100 epA where the signal from the Faraday cup was small compared to the electronic noise. So, in order to renormalize the cross section with a good Faraday cup measurement, in a second run at the same θ_{opt} the solid angle was reduced to 32 msr excluding the forward angles and increasing the beam current to measurable values. The beam current was optimized at each angle up to 10 enA in order to account for the strong dependence of the elastic scattering yield as a function of the ejectile angle. Under these conditions, an overlap of about 6° in the polar angle in the laboratory reference frame was achieved between adjacent runs. The overall measured angular range in the center-of-mass framework was $5^\circ \leqslant \theta_{c.m.} \leqslant 22^\circ$. The magnetic fields of the MAGNEX quadrupole and bending magnet were set in order to transport the $^{20}Ne^{10+}$ ions corresponding to elastic scattering events at the center of the focal plane detector (FPD) [30].

The data reduction strategy, including position calibration of the FPD, identification of the ejectiles of interest, and reconstruction of the momentum vector at the target by inversion of the transport equations followed the same method presented in previous publications [31–34]. This procedure also allows an accurate determination of the overall detection efficiency, as presented in Ref. [35], which is fundamental to extract the absolute cross section from the collected event yields.

In the present experimental conditions, the achieved angle and energy resolutions are $\delta\theta_{LAB}$(FWHM) $\sim 0.5^\circ$ and δE(FWHM) ~ 0.5 MeV, respectively. Figure 1 shows an example of excitation energy (E_x) spectrum for the ^{76}Ge(^{20}Ne, ^{20}Ne)^{76}Ge reaction obtained in the angular region between 13° and 15° in the laboratory reference frame. The first observed peak is described as the superposition of the ground state (g.s.) and the first 2^+ state of the ^{76}Ge at $E_x = 0.563$ MeV. The energy resolution is not enough to fully separate them, but the presence of the 2^+ state is important in order to reproduce the shape of the experimental data. A structure is present at $E_x \simeq 1.6$ MeV due to the sum of

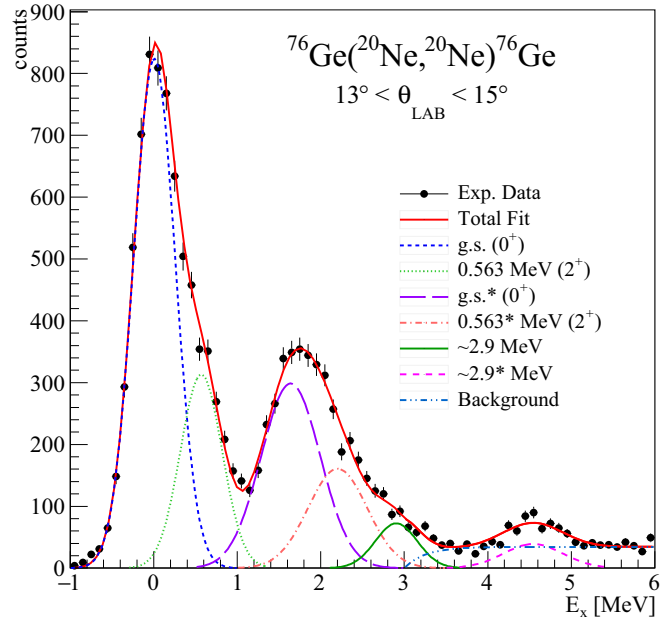

FIG. 1. Excitation energy spectrum of ^{76}Ge for the ^{20}Ne + ^{76}Ge elastic scattering at 306 MeV bombarding energy and $13^\circ < \theta_{lab} < 15^\circ$. Some peaks are identified in the figure by lines obtained fitting experimental data. Several states are expected to be populated starting from 3 MeV and are summarized in the fit by a unique background curve. In the legend, the curves marked by an asterisk correspond to states in which the ^{20}Ne is in the 2^+ state at 1.634 MeV.

different states where the dominant is the 2^+ excited state of projectile at $E_x = 1.634$ MeV. The contribution at $E_x = 0.563 + 1.634$ MeV corresponds to the excitation of the first 2^+ states of both target and projectile. Another state is present at $E_x \simeq 2.9$ MeV and also visible at $E_x \simeq 2.9 + 1.634$ MeV at the energy in which also the projectile is excited in its 2^+ first excited state. The width of this state is compatible with the 0^+ state of ^{76}Ge at 2.897 MeV already observed in (p, p') and (α, α') reactions [36]. A multiple-fit procedure was performed to describe the energy spectrum at several angles (see the example in Fig. 1) where the width of each peak was fixed according to the achieved energy resolution and the Doppler enlargement due to the in-flight decay of the projectile populated states. The contribution over 3 MeV in the excitation energy spectrum due to the weakly populated states of projectile and target is summarized in the fit procedure as a unique background curve.

Experimental angular distribution data for the different angular ranges are presented in Fig. 2. The statistical error and the uncertainties coming from the fitting procedure and from the differential solid angle evaluation are included in the error bars. A scale factor equal to 1.11 was applied to all the data to ensure a good agreement with the Rutherford cross section at very forward angles. This scale factor is compatible with the estimated systematic errors in the total charge collected by the Faraday cup and in the total number of scattering centers.

The 2^+ excited states of projectile (1.634 MeV) and target (0.563 MeV) were included in the coupling scheme

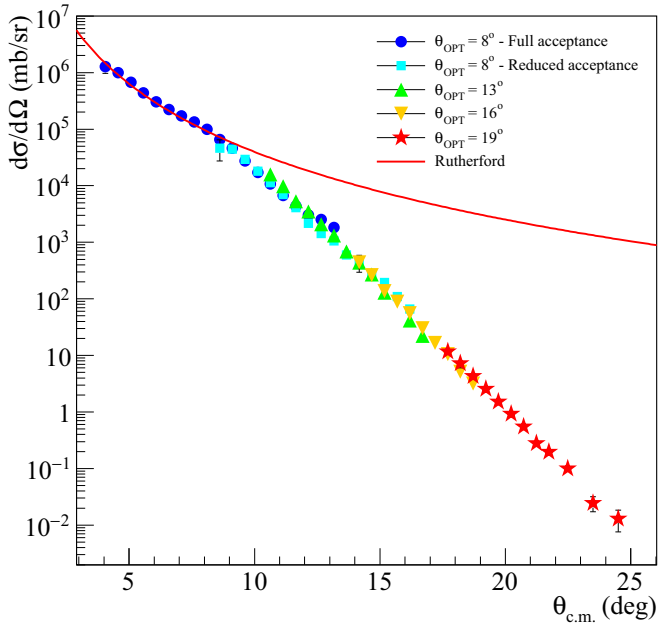

FIG. 2. Angular distribution of differential cross section for ^{20}Ne + ^{76}Ge elastic scattering at 306 MeV bombarding energy. Color points show data acquired in five separate runs for different angular settings (see text). The red line represents the Rutherford cross section.

shown in Fig. 3. The representation of the cross section in terms of the ratio to the Rutherford one (shown in Figs. 4 and 5) reveals a Fresnel-like scattering pattern, as expected for such heavy colliding nuclei (Sommerfeld parameter $\eta = 12.9$; grazing angular momentum $L_G \simeq 129\hbar$). The Coulomb field dominates the scattering up to the grazing angle, located at about $\theta_G \simeq 9.4^\circ$ in the c.m. reference frame, where the data show a Coulomb rainbow pattern. Beyond that angle, the data

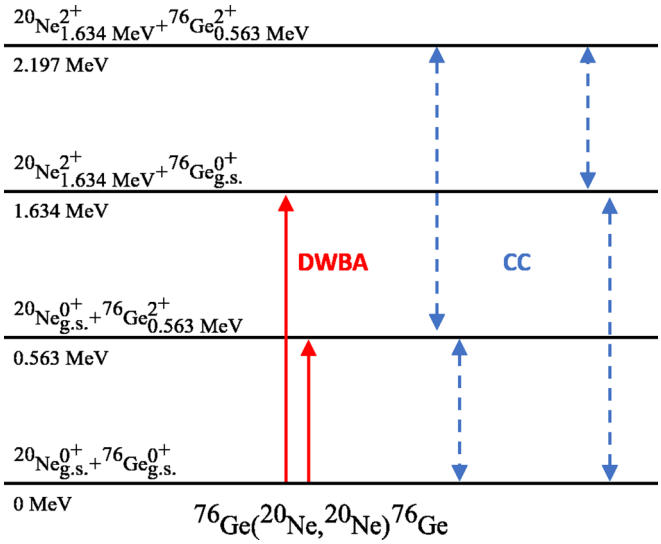

FIG. 3. Scheme of all the coupling potentials included in the DWBA and CC calculations among the different states of projectile and target.

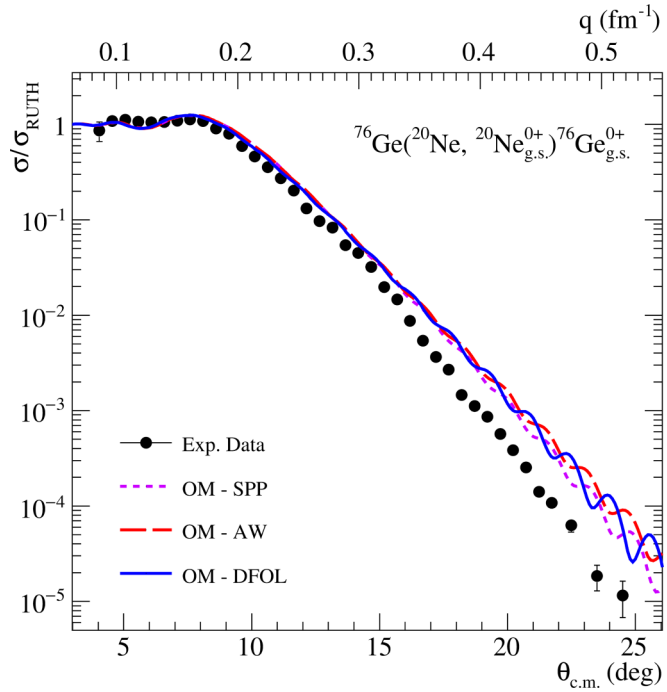

FIG. 4. Angular distribution of the elastic differential cross section in terms of its ratio with the Rutherford cross section σ_{RUTH}. Black dots are obtained from the coloured ones in Fig. 2 by an average weighted on the error of each measurement. Lines represent optical model calculations performed on the context of different optical potentials.

are more sensitive to the nuclear component of the nucleus-nucleus potential, showing the typical falloff associated with near and far-side scattering amplitudes. Differential cross-section angular distributions have been extracted also for the first 2^+ states of projectile, target, and simultaneous excitation of both of them, and these are shown in Fig. 6.

III. THEORETICAL ANALYSIS

The theoretical interpretation of angular distributions for the elastic and inelastic channels of the ^{20}Ne + ^{76}Ge collision was performed using FRESCO code [37]. The influence of the choice of different types of optical potentials was investigated by comparing the calculations obtained in the optical model (OM) with the angular distribution of elastic differential cross section. The inelastic differential cross sections can be obtained from DWBA calculations. The effect and strength of the coupling are evaluated by comparing these elastic and inelastic cross sections with those obtained by the CC technique.

A. Elastic scattering (study of the optical potential)

Usually, the elastic scattering can be described using a complex optical potential

$$U_{OPT}(r) = V(r) + iW(r) \quad (1)$$

in which the imaginary part $W(r)$ summarizes the nonelastic contributions in the average nucleus-nucleus interaction and

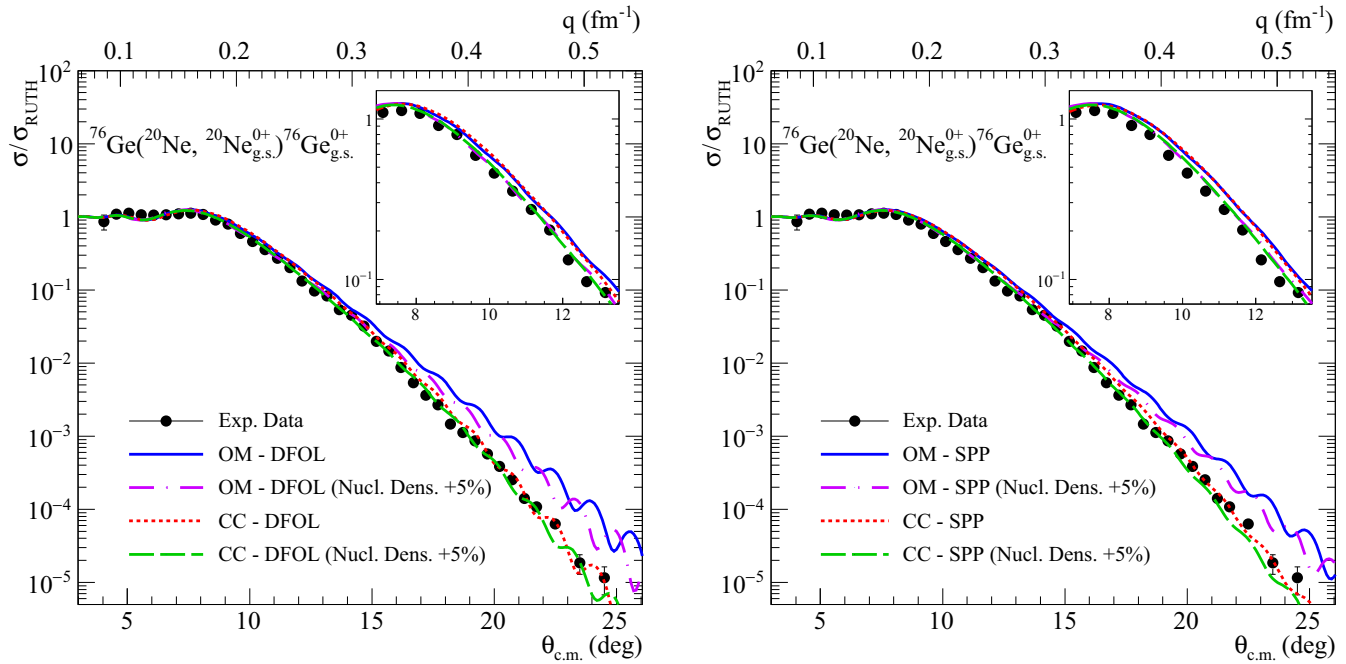

FIG. 5. Elastic scattering angular distributions of differential cross section in terms of the $\sigma/\sigma_{\mathrm{RUTH}}$ ratio. Panels (a) and (b) show the results obtained in OM and CC approaches with the DFOL and SPP double-folding potentials, respectively. In both panels, the solid blue and dot-dashed violet curves represent the OM calculations with the standard potentials and with +5% of the radius of the nuclear density distributions, respectively (see text). The red dotted and green dashed curves are the results of the CC approach obtained with the standard and the modified potentials.

results in an absorptive component for the elastic cross section. In the present work, three different optical potentials are tested: the parametric Akyuz-Whinter (AW) [22,23] and two double-folding optical potentials, the DFOL [26] and the São Paulo potential (SPP) [24,25].

The real part $V(r)$ of the AW potential is a central Woods-Saxon function in which radius R, strength V_0 and diffuseness a are extracted by the interpolation of double-folding potentials fitted on many nuclear systems in a quite large range of masses and energies. In the double-folding approach, V is obtained by the folding of the nucleon-nucleon interaction $V_{NN}(\mathbf{r}_1, \mathbf{r}_2, E)$ on the densities of the two involved nuclei $\rho_1(\mathbf{r}_1)$ and $\rho_2(\mathbf{r}_2)$:

$$V(r) = \int d\mathbf{r}_1 d\mathbf{r}_2 \rho_1(\mathbf{r}_1)\rho_2(\mathbf{r}_2)V_{NN}(\mathbf{r}_1, \mathbf{r}_2, E), \qquad (2)$$

where r is the projectile-target distance and E is the energy per nucleon in the center-of-mass reference frame.

The densities $\rho_j(\mathbf{r}_j)$ of projectile and target used in the foldings of both SPP and DFOL potentials are parametrized by Wood-Saxon profiles. Density parameters used in the SPP and DFOL folding are taken from Refs. [24] and [26], respectively. In the DFOL approach, the T-matrix interaction at $E_{\mathrm{lab}} = 50$ MeV from Ref. [27] was used to calculate the real and imaginary parts of the optical potential through the same procedure described in Ref. [38]. The imaginary parts of the AW and SPP optical potentials were obtained from the real ones scaling their strength by a factor 0.78, as also seen in previous works of Refs. [39–42], and a 0.8 scale factor was applied also to the DFOL optical potential.

The results of OM calculations performed with the three tested optical potentials and the experimental data in the $\sigma/\sigma_{\mathrm{RUTH}}$ representation are shown in Fig. 4. There is not a significant difference between the three calculations. This fact confirms that the theoretical description of elastic scattering is not strongly dependent on the choice of the optical potential since the strong absorption confines the reaction source on the surface of the colliding systems. Although different in terms of root main square radius and volume integral per nucleon, the total reaction cross section (see Table I) and the angular distribution (see Fig. 4) are very similar for all the studied potentials.

In Fig. 4, the experimental data beyond the grazing angle (≈9.4°) show a slope steeper than that obtained from our OM calculations. Since all of them, performed with different

TABLE I. Total reaction cross sections σ_R, volume integral per nucleon J, and root mean square radii $\sqrt{\langle R^2 \rangle}$ for the real (V) and imaginary (W) parts of the AW, DFOL, and SPP potentials.

	σ_R (mb)	J_V (MeV fm^3)	J_W (MeV fm^3)	$\sqrt{\langle R_V^2 \rangle}$ (fm)	$\sqrt{\langle R_W^2 \rangle}$ (fm)
AW	2807	−1390	−1042	7.03	7.03
DFOL	2819	−6928	−5108	5.30	5.18
SPP	2799	−5426	−4069	5.32	5.32

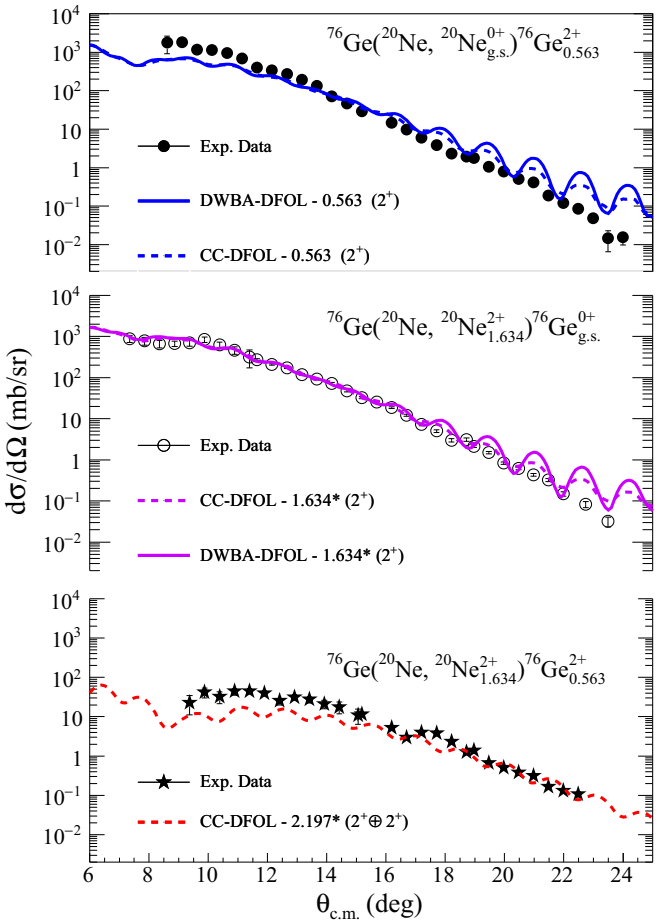

FIG. 6. Angular distribution of differential cross section for the low-lying states of projectile and target populated in the ^{20}Ne + ^{76}Ge inelastic scattering at 306-MeV bombarding energy: in the top panel, 2^+ state of ^{76}Ge at 0.563 MeV; in the middle panel, the 2^+ state of the ^{20}Ne at 1.634 MeV; in the bottom panel, the 2.197-MeV state that corresponds to the excitation of both projectile and target $2^+ \oplus 2^+$. Solid lines are the results obtained in DWBA approach; dashed lines are CC calculations.

potentials, are in agreement with each other, the discrepancy could indicate a common drawback in the description of the geometrical properties of the nuclear densities. An important approximation is that the density profiles used in the folding of the DFOL and SPP optical potentials for both projectile and target isotopes that are assumed to be spherical. Moreover, the AW optical potential parameters are obtained from interpolations of double-folding optical potentials of several nuclear systems in a quite large range of energies and masses. Also, in this case the nuclear systems are assumed to be spherical.

Since both ground-state (g.s.) quadrupole moments of projectile and target are large [43], one has to infer that ^{20}Ne and ^{76}Ge isotopes are significantly deformed. Moreover, at these transferred momenta, the hypothesis of *frozen* nuclear spherical matter in the reaction mechanism is not enough supported. An effective way to take these arguments into account in the building of the optical potential is to change the density matter profiles used in the folding of the *NN* interactions, as also described in Refs. [44–46]. Nevertheless, a renormalization is mandatory in order to keep constant the volume integral of the nuclear densities to fix the number of nucleons.

In the present work, this operation has been performed by increasing the radius of the nuclear density profiles by 5% in the folding of both the DFOL and the SPP optical potentials and renormalizing the central density parameter. The comparison between the standard approach and the new one is shown in Fig. 5 by the solid blue and dot-dashed violet curves. The increase of radius appears important to correctly describe the experimental shape up to about 14°, where geometrical properties of nuclei are more relevant. However, the change of slope observed in the experimental data above 14° is still not described in the OM framework.

The effect in the elastic channel of the inclusion of couplings with the first low-lying excited states of projectile and target is shown in Fig. 5 by the red-dotted and green dashed curves for both the double-folding potentials (DFOL and SPP). This effect is here evaluated also in terms of the transferred momentum q, calculated by the approximated expression $\approx 2E_{c.m.}/\hbar c \sin\theta_{c.m.}$. The effect of couplings starts to be important in the description of the elastic scattering over 15°, at almost 0.3 fm^{-1}, where the absolute cross sections for the elastic and the inelastic scattering channels become comparable. Other details on the performed CC calculations are described in the next subsection.

B. Inelastic scattering (study of coupling contributions)

The angular distributions of the transition to the first excited states of the projectile (2^+ at 1.634 MeV), target (2^+ at 0.563 MeV), and simultaneous excitation of both ($2^+ \oplus 2^+$ at 2.197 MeV) are shown in Fig. 6. Calculations for the excited states were performed in DWBA and CC approaches in the context of a rotational model in which the 2^+ states are treated as quadrupole excitations of pure rotors. Coulomb deformations of nuclei were introduced in terms of reduced transition probabilities. $B(E2;\ 0^+ \rightarrow 2^+) = 0.0333\,\mathrm{e^2b^2}$ for ^{20}Ne and $B(E2;\ 0^+ \rightarrow 2^+) = 0.2735\,\mathrm{e^2b^2}$ for ^{76}Ge are obtained from Ref. [43] and were used to describe Coulomb deformations of both projectile and target. The $V_2^i(r)$ nuclear coupling potentials are treated in the first-order approximation described in Ref. [12] through the following formula:

$$V_2^i(r) = -\frac{\delta_2^i}{\sqrt{4\pi}}\frac{dU(r)}{dr}, \tag{3}$$

where the deformation lengths $\delta_2^i = \beta_2^i R^i$ are calculated through the deformations β_2^i and radii R_i of each nucleus indicated by i. For the imaginary coupling potentials, the same radial form factors are assumed taking the $\beta_2^{\mathrm{real}} = \beta_2^{\mathrm{imag}}$ convention. Calculations shown in Fig. 6 have been performed using only the DFOL optical potential since the results obtained with the SPP are in complete agreement with them. The DFOL optical potential is the one obtained by increasing the radius of Woods-Saxon nuclear density profiles of 5% to ensure a good agreement with elastic scattering data at forward angles, as previously described in Sec. III A.

Calculations for the first low-lying excited states are in a reasonable agreement with experimental data. The effect of higher order terms of couplings to the elastic channel is not relevant in the description of the average shape of the angular distributions for the inelastic transitions, as shown in the top and middle panels of Fig. 6. Here, the main effect of couplings is a smoothing in the oscillation pattern over 16°, also present in the data. A description of the angular distribution for the $2^+ \oplus 2^+$ state at 2.197 MeV is not possible in the DWBA one-step approach since the relative transition is a second-order process (see Fig. 3). The CC calculation performed is shown in the bottom panel of Fig. 6, and the obtained result is in good agreement with the experimental data.

IV. CONCLUSIONS

In the present work, elastic and inelastic scattering of the ^{20}Ne + ^{76}Ge at 306 MeV were studied for the first time, including good theoretical descriptions of their excitations by using optical model and CC approaches. The g.s. to g.s. transition was separated by the other inelastic channels thanks to the very good resolution gained through a careful tuning of the experimental setup and the applied advanced analysis. Moreover, the small error bars and the overall quality of the experimental data justify the attempt to use sophisticated microscopic analysis.

The capability of several optical potentials to fit the angular distribution of the measured differential cross sections was tested, showing that the responses with the AW optical potential and the SPP and DFOL double-folding potentials are practically the same. Standard versions of all these potentials were not enough to correctly describe the experimental data above the grazing angles. This goal was partially achieved by working on the geometrical parameters of the nuclear matter densities of isotopes involved. Since both the ^{20}Ne and ^{76}Ge are deformed, an effective way to take this property into account is to increase the radius of their nuclear matter densities by 5%, thus obtaining good agreement until about 14° in the elastic scattering angular distribution.

At transferred momentum greater than 0.3 fm^{-1}, the effect of couplings with first low-lying excited states becomes essential to describe especially the elastic scattering where the cross section becomes comparable with the ones of first 2^+ states. Other studies have to be performed in order to check if contributions from coupling to the projectile and target 2^+ low-lying states are relevant to the DCE and SCE reaction cross sections. In this context, new analyses have to be performed in order to find the appropriate characterization of the model space and average interaction for the outgoing partition.

ACKNOWLEDGMENTS

This project has received funding from the European Research Council (ERC) under the European Union's Horizon 2020 research and innovation programme (Grant Agreement No. 714625) and from the Mexican grants DGAPA-PAPIIT sIG101016, IA103218, PIIF2018 and CONACyT 294537. J.A.L. acknowledges funding from the European Union's Horizon 2020 research and innovation programme under Grant Agreement No. 654002 and from the Spanish Ministerio de Economia y Competitividad and FEDER funds under Project No. FIS2017-88410-P.

[1] S. Dell'Oro, S. Marcocci, and F. Vissani, Phys. Rev. D **90**, 033005 (2014).
[2] F. Cappuzzello, C. Agodi, M. Cavallaro, D. Carbone, S. Tudisco, D. Lo Presti, J. R. B. Oliveira, P. Finocchiaro, M. Colonna, D. Rifuggiato *et al.*, Eur. Phys. J. A **54**, 72 (2018).
[3] F. Cappuzzello, C. Agodi, M. Bondì, D. Carbone, M. Cavallaro, and A. Foti, J. Phys.: Conf. Ser. **630**, 012018 (2015).
[4] H. Matsubara, M. Takaki, T. Uesaka, S. Shimoura, N. Aoi, M. Dozono, T. Fujii, K. Hatanaka, T. Hashimoto, T. Kawabata *et al.*, Few-Body Syst. **54**, 1433 (2013).
[5] K. Kisamori, S. Shimoura, H. Miya, S. Michimasa, S. Ota, M. Assie, H. Baba, T. Baba, D. Beaumel, M. Dozono *et al.*, Phys. Rev. Lett. **116**, 052501 (2016).
[6] K. Takahisa, H. Ejiri, H. Akimune, H. Fujita, R. Matumiya, T. Ohta, T. Shima, M. Tanaka, and M. Yosoi, arXiv:1703.08264.
[7] N. Shimizu, J. Menéndez, and K. Yako, Phys. Rev. Lett. **120**, 142502 (2018).
[8] H. Lenske, J. I. Bellone, M. Colonna, and J. A. Lay, Phys. Rev. C **98**, 044620 (2018).
[9] H. Lenske, J. Phys.: Conf. Ser. **1056**, 012030 (2018).
[10] M. Colonna, J. I. Bellone, S. Burrello, J. A. Lay, and H. Lenske, in *Proceedings of the 15th International Conference on Nuclear Reaction Mechanisms, Varenna, Italy, June 11–15, 2018* (CERN, Geneva, 2019), Vol. 1.
[11] A. Kumar, R. Kanungo, A. Calci, P. Navrátil, A. Sanetullaev, M. Alcorta, V. Bildstein, G. Christian, B. Davids, J. Dohet-Eraly *et al.*, Phys. Rev. Lett. **118**, 262502 (2017).
[12] G. R. Satchler, *Direct Nuclear Reactions*, International Series of Monographs on Physics Vol. 68 (Clarendon Press, Oxford, UK, 1983).
[13] G. R. Satchler and W. G. Love, Phys. Rep. **55**, 183 (1979).
[14] O. Sgouros, V. Soukeras, A. Pakou, N. Patronis, K. Zerva, N. Keeley, I. Strojek, A. Trzcińska, E. Piasecki, K. Rusek *et al.*, Int. J. Mod. Phys. E **22**, 1350073 (2013).
[15] A. Trzcińska, E. Piasecki, K. Hagino, W. Czarnacki, P. Decowski, N. Keeley, M. Kisieliński, P. Koczoń, A. Kordyasz, E. Koshchiy *et al.*, Phys. Rev. C **92**, 034619 (2015).
[16] S. Ohkubo and Y. Hirabayashi, Phys. Rev. C **89**, 051601(R) (2014).
[17] S. Ohkubo and K. Yamashita, Phys. Rev. C **66**, 021301(R) (2002).
[18] V. A. B. Zagatto, F. Cappuzzello, J. Lubian, M. Cavallaro, R. Linares, D. Carbone, C. Agodi, A. Foti, S. Tudisco, J. S. Wang *et al.*, Phys. Rev. C **97**, 054608 (2018).
[19] D. Pereira, R. Linares, J. R. B. Oliveira, J. Lubian, L. C. Chamon, P. R. S. Gomes, A. Cunsolo, F. Cappuzzello, M. Cavallaro, D. Carbone *et al.*, Phys. Lett. B **710**, 426 (2012).

[20] J. R. B. Oliveira, F. Cappuzzello, L. C. Chamon, D. Pereira, C. Agodi, M. Bondí, D. Carbone, M. Cavallaro, A. Cunsolo, M. De Napoli *et al.*, J. Phys. G: Nucl. Part. Phys. **40**, 105101 (2013).
[21] F. Cappuzzello, D. Nicolosi, R. Linares, J. R. B. Oliveira, J. Lubian, C. Agodi, D. Carbone, M. Cavallaro, P. N. de Faria, A. Foti *et al.*, Eur. Phys. J. A **52**, 169 (2016).
[22] R. O. Akyuz and A. Winther, in *Proceedings of the Enrico Fermi International School of Physics*, edited by R. A. Broglia, C. H. Dasso, and R. Ricci (North-Holland, Amsterdam, 1979).
[23] R. A. Broglia and A. Winther, *Heavy Ion Reactions*, Lecture Notes on the Elementary Processes, Frontiers in Physics (Addison Wesley Publishing Company, New York, 1991).
[24] L. C. Chamon, B. V. Carlson, L. R. Gasques, D. Pereira, C. De Conti, M. A. G. Alvarez, M. S. Hussein, M. A. Candido Ribeiro, E. S. Rossi, Jr., and C. P. Silva, Phys. Rev. C **66**, 014610 (2002).
[25] D. Pereira, J. Lubian, J. R. B. Oliveira, D. P. de Sousa, and L. C. Chamon, Phys. Lett. B **670**, 330 (2009).
[26] H. Lenske (private communication).
[27] M. A. Franey and W. G. Love, Phys. Rev. C **31**, 488 (1985).
[28] L. Rifuggiato, D. Calabretta, and G. Cuttone, in *Cyclotrons and Their Applications: Proceedings of the 17th International Conference, Cyclotrons 2004*, edited by A. Goto (Particle Accelerator Society of Japan, Tokyo, 2004).
[29] F. Cappuzzello, C. Agodi, D. Carbone, and M. Cavallaro, Eur. Phys. J. A **52**, 167 (2016).
[30] M. Cavallaro, F. Cappuzzello, D. Carbone, A. Cunsolo, A. Foti, A. Khouaja, M. R. D. Rodrigues, J. S. Winfield, and M. Bondì, Eur. Phys. J. A **48**, 59 (2012).
[31] F. Cappuzzello, M. Cavallaro, A. Cunsolo, A. Foti, D. Carbone, S. E. A. Orrigo, and M. R. D. Rodrigues, Nucl. Instrum. Meth. A **621**, 419 (2010).
[32] F. Cappuzzello, D. Carbone, and M. Cavallaro, Nucl. Instrum. Methods Phys. Res. A **638**, 74 (2011).
[33] S. Calabrese, F. Cappuzzello, D. Carbone, M. Cavallaro, C. Agodi, L. Acosta, D. Bonanno, D. Bongiovanni, T. Borello-Lewin, I. Boztosun *et al.*, Acta Phys. Polon. B **49**, 275 (2018).
[34] M. Cavallaro, G. Santagati, F. Cappuzzello, D. Carbone, R. Linares, D. Torresi, L. Acosta, C. Agodi, D. Bonanno, D. Bongiovanni *et al.*, Res. Phys. **13**, 102191 (2019).
[35] M. Cavallaro, F. Cappuzzello, D. Carbone, A. Cunsolo, A. Foti, and R. Linares, Nucl. Instrum. Meth. A **637**, 77 (2011).
[36] B. Singh, Nucl. Data Sheets **74**, 63 (1995).
[37] I. J. Thompson, Comput. Phys. Rep. **7**, 167 (1988).
[38] F. Cappuzzello, H. Lenske, A. Cunsolo, D. Beaumel, S. Fortier, A. Foti, A. Lazzaro, C. Nociforo, S. E. A. Orrigo, and J. S. Winfield, Nucl. Phys. A **739**, 30 (2004).
[39] M. J. Ermamatov, F. Cappuzzello, J. Lubian, M. Cubero, C. Agodi, D. Carbone, M. Cavallaro, J. L. Ferreira, A. Foti, V. N. Garcia *et al.*, Phys. Rev. C **94**, 024610 (2016).
[40] D. Carbone, J. L. Ferreira, F. Cappuzzello, J. Lubian, C. Agodi, M. Cavallaro, A. Foti, A. Gargano, S. M. Lenzi, R. Linares *et al.*, Phys. Rev. C **95**, 034603 (2017).
[41] M. J. Ermamatov, R. Linares, J. Lubian, J. L. Ferreira, F. Cappuzzello, D. Carbone, M. Cavallaro, M. Cubero, P. N. de Faria, A. Foti *et al.*, Phys. Rev. C **96**, 044603 (2017).
[42] B. Paes, G. Santagati, R. Magana Vsevolodovna, F. Cappuzzello, D. Carbone, E. N. Cardozo, M. Cavallaro, H. García-Tecocoatzi, A. Gargano, J. L. Ferreira *et al.*, Phys. Rev. C **96**, 044612 (2017).
[43] B. Pritychenko, M. Birch, B. Singh, and M. Horoi, At. Data Nucl. Data Tables **107**, 1 (2016).
[44] L. M. Fonseca, R. Linares, V. A. B. Zagatto, F. Cappuzzello, D. Carbone, M. Cavallaro, C. Agodi, J. Lubian, and J. R. B. Oliveira, Phys. Rev. C **100**, 014604 (2019).
[45] E. Crema, D. R. Otomar, R. F. Simões, A. Barioni, D. S. Monteiro, L. K. Ono, J. M. B. Shorto, J. Lubian, and P. R. S. Gomes, Phys. Rev. C **84**, 024601 (2011).
[46] E. Crema, V. A. B. Zagatto, J. M. B. Shorto, B. Paes, J. Lubian, R. F. Simões, D. S. Monteiro, J. F. P. Huiza, N. Added, M. C. Morais *et al.*, Phys. Rev. C **98**, 044614 (2018).